

X-ray Diffraction Investigation of Annealing Behavior of Peened Surface Deformation Layer on Precipitation Hardening Stainless Steel

Junjie Huang, Zhou Wang, Jin Gan, Ying Yang, Feng Huang, Gang Wu, and Qingshuai Meng

(Submitted July 18, 2017; in revised form November 9, 2017; published online April 2, 2018)

In order to investigate the recrystallization behavior of peened surface deformation layer of precipitation hardening stainless steel, a classic x-ray diffraction line profile analysis, Voigt method, was carried out on peened 17-4PH with different isothermal annealing temperatures. The activation energy of domain boundary migration (Q_a) and the activation energy of microstrain relaxation (Q_b) were calculated by regression analysis in different annealing temperature conditions. The results show that the value of Q_a decreases with annealing temperature increasing, which is due to the influence of precipitation (ϵ -Cu) size on the movements of grain and subgrain boundaries. The maximum growth rate of ϵ -Cu particles occurs during 400 to 500 °C interval. Compared with growth behavior of domain size, microstrain relaxation behavior is less sensitive to precipitation particle size. The effects of annealing temperature and time on dislocation density are both significant when annealing temperature is lower than 500 °C. However, the effect of annealing temperature on dislocation density becomes insignificant when annealing temperature is higher than 500 °C. 300 °C annealing temperature only leads to the microstrain relaxation but nearly cannot lead to the domain size growth even if prolonging annealing time. Microstructure enhancement effect still exists in plastic deformation layer when 300 °C annealing temperature lasts for 60 min but nearly disappears when 600 °C annealing temperature lasts for 20 min.

Keywords dislocation density, precipitation hardening stainless steel, recrystallization behavior, shot peening, Voigt method

1. Introduction

Precipitation hardening stainless steels have become increasingly important in industrial applications due to their excellent combination of mechanical properties and corrosion resistance (Ref 1-3). In order to improve the fatigue strength, stress corrosion resistance and surface hardness of precipitation hardening stainless steel, shot peening (SP) treatment is usually carried out on this kind of material (Ref 4,5). Two kinds of changes take place in surface deformation layer after SP treatment: the change of microstructure (such as domain size, microstrain and dislocation density) and the change of residual stresses. Both of these changes affect the fatigue properties of metals at room and elevated temperature. As the working temperature of precipitation hardening stainless steel component is usually higher than room temperature, the stabilities of residual stresses and microstructure in surface deformation

layer are very important for SP component in industry. Most of the researchers believe that the main reason of SP to improve fatigue resistance of material is due to introducing compressive residual stresses in the surface layer, which can hinder the nucleation and the propagation of fatigue cracks. Therefore, there are many research works regarding thermal relaxation of residual stresses in SP material (Ref 6-8), but the research works regarding the microstructure evolution of SP material at elevated temperature are rare (Ref 9). The investigation on the thermostability of microstructure at elevated temperatures is important for precipitation hardening stainless steels to maintain good fatigue properties, which is also a necessary complement to the previous work (Ref 6). Until now, most of the researches about precipitation hardening stainless steels focus on the mechanical properties during aging kinetics (Ref 1,10-12), and little investigation has been carried out on recrystallization behavior and microstructure thermostability of precipitation hardening stainless steels after cold work hardening treatment such as SP.

X-ray diffraction line profile analysis is a powerful alternative to electron microscope for characterizing the microstructure of crystalline materials because of reliability and non-destruction (Ref 9,13-15). Moreover, compared with SEM, TEM or other electron microscope's results, the microstructure obtained from x-ray diffraction is a statistical result which can reflect the average case of microstructure in relative large area. To some extent, the microstructure obtained from x-ray diffraction measurement is more meaningful for material overall mechanical properties than electron microscope's results. In this paper, one typical precipitation hardening stainless steel, 17-4PH, was chosen as investigated material. This kind of steel is widely used in industry for a variety of applications including turbine blades, gears, nuclear reactor

Junjie Huang, Nanjing Center, China Geological Survey, Nanjing 210016 Jiangsu, People's Republic of China; **Zhou Wang**, **Ying Yang**, **Feng Huang**, **Gang Wu**, and **Qingshuai Meng**, School of Automotive Engineering, Wuhan University of Technology, Wuhan 430070 Hubei, People's Republic of China; and Hubei Key Laboratory of Advanced Technology of Automotive Components, Wuhan University of Technology, Wuhan 430070 Hubei, People's Republic of China; and **Jin Gan**, School of Transportation, Wuhan University of Technology, Wuhan 430063 Hubei, People's Republic of China. Contact e-mail: wangzhou@whut.edu.cn.

components (Ref 1). The recrystallization behavior of deformation layer induced by SP was discussed via XRD line profile analysis.

2. Experimental Setup

Investigations were carried out on 17-4PH steel specimens. The chemical composition of 17-4PH steel is listed in Table 1. The specific heat treatment process was austenitized for 1 h at 1035 °C, water quenched down to 25 °C, tempered at 815 °C for 0.5 h and cooled in a vacuum furnace, tempered again at 570 °C for 3 h and cooled in a vacuum furnace. The dimensions of all specimens were 30 mm × 15 mm × 10 mm. In this work, the dual SP treatment was carried out on 30 mm × 15 mm surface of all specimens via air blast SP equipment. The shot media of the first and the second SP treatments were cast steel balls ($D_{\text{diameter}} = 1.0$ mm, 640 HV) and Al₂O₃ ceramic balls ($D_{\text{diameter}} = 0.1$ mm, 700 HV), respectively. The diameter of peening nozzle was 15 mm, and the distance from peening nozzle to specimen was 100 mm. The shots impact angle was 90°. A type Almen strips were used to measure peening intensities, and the arc height of Almen specimen was 0.5 + 0.1 mmA for all specimens in this work.

In order to investigate the recrystallization behavior of peened 17-4PH, the different isothermal annealing processes were carried out with temperatures ranging from 300 to 600 °C. XRD investigation was conducted on the SP specimens after the specimens cooled down to room temperature. The microstructure variations of deformation layer were calculated by a classic XRD line profile analysis method: Voigt method (Ref 16,17). According to Voigt method, the observed XRD line profile $h(x)$ can be expressed as after Stokes deconvolution (Ref 18):

$$h(x) = \int_{-\infty}^{+\infty} g(y)f(x-y)dy \quad (\text{Eq 1})$$

where f is the structurally broadened profile and g is the instrumental profile. According to Voigt method, the relationship of integral breadth β is given by (Ref 16,17):

$$\beta_G^h = \beta_G^f + \beta_G^g, \beta_C^h = \beta_C^f + \beta_C^g \quad (\text{Eq 2})$$

where subscripts G and C denote the Gaussian and Cauchy components, and superscripts h, f, g denote the measured line profile, the structurally broadened profile and the instrumental profile, respectively. It is assumed that the Cauchy component of the f profile is solely due to crystallite size and the Gaussian component of the f profile is solely due to microstrain. In Voigt method, the domain size and microstrain are given by (Ref 16,17):

$$D = \lambda / \beta_C^f \cos(\theta), \varepsilon = \beta_G^f / 4 \tan(\theta) \quad (\text{Eq 3})$$

In order to calculate the variation of the domain size and microstrain during isothermal annealing, (110) crystallite plane of 17-4PH steel and α -Fe annealed powder were measured as the h and the g profiles. The diffraction profiles of all specimens were measured by Dmax/rc diffractometer with CuK α radiation, voltage 40 kV and current 100 mA. The scan velocity was 0.5°/min, and the step size was 0.01°.

For the calculation of dislocation density, the relationship between dislocation density, domain size and microstrain is accordingly given by (Ref 19,20):

$$\rho_t = \frac{2\sqrt{3}}{b} \cdot \frac{\langle \varepsilon^2 \rangle^{1/2}}{L} \quad (\text{Eq 4})$$

where ρ_t is the total dislocation density, b is the amount of the burgers vector of dislocation [$b = 0.25$ nm in this work (Ref 5)], L is the mean domain size in specific direction (size of coherent scattering regions), and $\langle \varepsilon^2 \rangle^{1/2}$ is the mean microstrain.

As SP treatment leads to some microdefects existing on the surface of specimen, the XRD measurements were taken on specimens after the removal of 20- μ m layer from peened surface via electrolytic method in order to avoid the microdefect effect. The exact removal depth was measured and controlled via vernier caliper. In this paper, all the data of peened surface were 20 μ m from real surface. The depth profiles of microstructure calculated values were determined by iterative electrolytic removal of thin surface and subsequent x-ray measurement.

3. Results and Discussion

In the SP treatment, both of new residual stresses distribution and microstructure variations are introduced into the near-surface region. Figure 1 shows the XRD patterns of the peened surface under different annealing time and temperature conditions. The characteristic peaks of base material (α -Fe) and the phase that precipitates from the matrix (ε -Cu) appear in all annealing conditions. From Fig. 1(a), it can be seen that all α -Fe diffraction peaks become sharper with time increasing in the 300 °C annealing temperature condition. From Fig. 1(b), it can be seen that all α -Fe diffraction peaks become sharper with annealing temperature increasing in the condition of 60-min annealing time. As SP treatment leads to the domain size decreasing and microstrain increasing in the surface deformation layer (Ref 21-23), recrystallization behavior of surface deformation layer definitely occurs when annealing process is carried out on SP specimens.

Table 1 The chemical composition of 17-4PH

Element composition, wt.%						
C	Si	Mn	Cr	Ni	Cu	Nb + Ta
≤ 0.055	≤ 1.00	≤ 0.5	15.00-16.00	3.80-4.50	3.00-3.70	0.15-0.35
P	S	Al	Ti	N	Fe	...
≤ 0.035	≤ 0.030	≤ 0.050	≤ 0.05	≤ 0.05	Balance	...

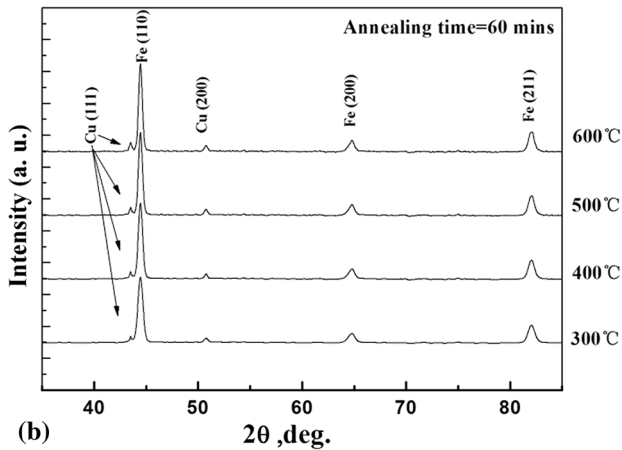
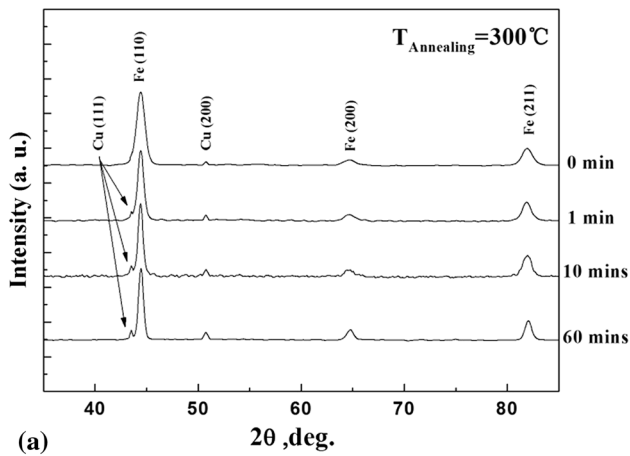


Fig. 1 XRD patterns of peened 17-4PH surface with different annealing times and temperatures (a) $T_{\text{annealing}} = 300\text{ }^{\circ}\text{C}$; (b) annealing time = 60 min

In order to obtain the evolution of domain size and microstrain of peened 17-4PH during annealing process, the structurally broadened profiles of 17-4PH peened specimens were separated from observed XRD line profile firstly by Eq 1 and 2 according to XRD pattern shown in Fig. 1. After that the domain size and microstrain in different annealing conditions were calculated by Eq 3 according to the data from obtained Gaussian and Cauchy integral breadth β . Figure 2 shows the evolution of surface domain size in different annealing temperature conditions. It can be seen that the nanoscaled domain size appeared at the top surface after the SP treatment and the domain size increases with annealing time increasing. Higher annealing temperature makes the domain growth rate faster. Comparing with the growth behavior of domain size in this four annealing temperature conditions, it can be seen that the domain growth rate is higher in the initial stage of annealing (5 min). This phenomenon is more obvious under the condition of higher-temperature annealing process. With increasing annealing time, the domain growth rate becomes lower. Specifically, the domain growth rates of 300 and 600 °C annealing temperatures are 1.2 and 15.2 nm/min in the initial stage of annealing process; meanwhile, the domain growth rates of 300 and 600 °C annealing temperature are 0.5 nm/min and 4.1 nm/min when annealing time is about 60 min. The growth rate of domain size D can be given by (Ref 24):

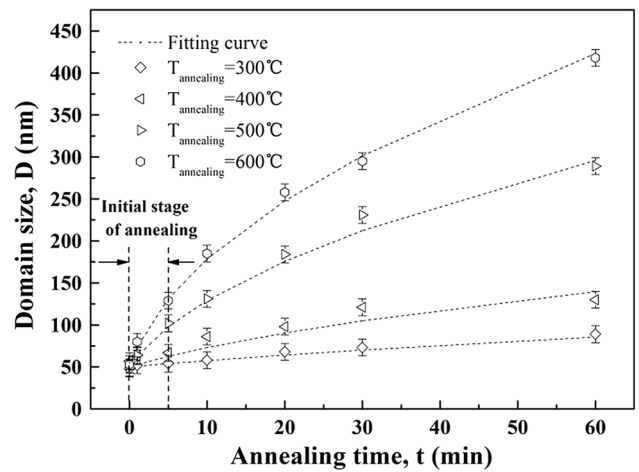


Fig. 2 The evolution of surface domain size in different annealing temperature conditions

$$\frac{dD}{dt} = AD^{-n} \exp\left[-\frac{Q_a}{RT}\right] \quad (\text{Eq 5})$$

where t is the annealing time, T is the annealing temperature, R is the gas constant ($8.314\text{ J}\cdot\text{mol}^{-1}\cdot\text{K}^{-1}$), A and n are the material's constants, and Q_a is the activation energy of domain boundary migration. Integrating D in Eq 5 can give:

$$D_t^2 = D_0^2 + At(n+1) \exp\left[-\frac{Q_a}{RT}\right] \quad (\text{Eq 6})$$

where D_0 is the original domain size and D_t is the domain size at t time. According to Eq 6 and the data in Fig. 2, the values of Q_a in annealing temperatures 300, 400, 500 and 600 °C are obtained by computer regression analysis, which are 40.2, 40.0, 35.8 and 35.1 kJ/mol, respectively. According to the calculated results, Q_a decreases with increasing temperature of annealing process, but the variation of Q_a is insignificant when the annealing temperature is below 400 °C or above 500 °C, which is mainly due to the influence of precipitation on the movements of grain and subgrain boundaries. It is well known that the hardening mechanism of 17-4PH is due to the formation of a submicroscopic copper-rich phase, so the precipitation particles of copper play an important role in the recrystallization behavior. In the early stage of the precipitation of copper, coherent bcc clusters nucleate and grow in the supersaturated bcc matrix and lose coherency after reaching a certain critical size (Ref 1,25, 26). After that, the size of particle (ϵ -Cu) increases with the annealing time. According to the calculated data, activation energy of domain boundary migration decreases with temperature increasing in the range from 300 to 600 °C, which represents the dislocations movement of peened 17-4PH in lower-temperature annealing process is more difficult than that in higher-temperature annealing process. Specifically, Q_a decreases only about 0.2 kJ/mol when annealing temperature increases from 300 to 400 °C but decreases 4.4 kJ/mol when annealing temperature increases from 400 to 500 °C, which represents the size of precipitation particles (ϵ -Cu) increases insignificantly during 300 to 400 °C but increases sharply in the range of 400 to 500 °C. The Q_a decreases 0.7 kJ/mol from 500 to 600 °C, which represents the growth rate becomes lower again in the range of 500-600 °C.

According to Ref 24, 27, there are two mechanisms for precipitation hardening, i.e., dislocations cutting through particle mechanism and dislocations bowing around particle mechanism, which depends on the size of the precipitate particles. The schematic diagram of precipitation hardening mechanism is shown in Fig. 3. In terms of dislocation cutting through particle mechanism, as the size of the second-phase particles increases, the particles impede dislocation movement and it becomes increasingly difficult for the particles to cut through the material. The material strength can be given as Eq 7:

$$\tau = \frac{\pi r \gamma}{bL} \quad (\text{Eq 7})$$

where τ is material strength, r is the second-phase particle radius, γ is the surface energy, b is the magnitude of the Burgers vector, and L is the spacing between pinning points. From this equation, it can be seen that the strength of a material increases with increasing r . In terms of dislocations bowing around particle mechanism, the strength is inversely proportional to the second-phase particle radius r , which can be given as Eq 8:

$$\tau = \frac{Gb}{L - 2r} \quad (\text{Eq 8})$$

where τ is the material strength, G is the shear modulus, b is the magnitude of the Burgers vector, L is the distance between pinning points, and r is the second-phase particle radius. Dislocation bowing, also called Orowan strengthening (Ref 27), is more likely to occur when there are large particles present in the material. When r is smaller than critical radius, cutting mechanism will dominate. When r is larger than critical radius, bowing mechanism will dominate.

According to Ref 1, 6, the critical radius of age-hardening 17-4PH appears in the condition of tempered at 480 °C for 1 h. The critical radius of the second-phase particle (ϵ -Cu) leads to maximum strength and hardness occurring in this condition. As the initial condition of 17-4PH specimen in this work was tempered 815 °C for 0.5 h and tempered again at 570 °C for 3 h, the radius of the second-phase particle (ϵ -Cu) must be larger than critical radius. The precipitation hardening mech-

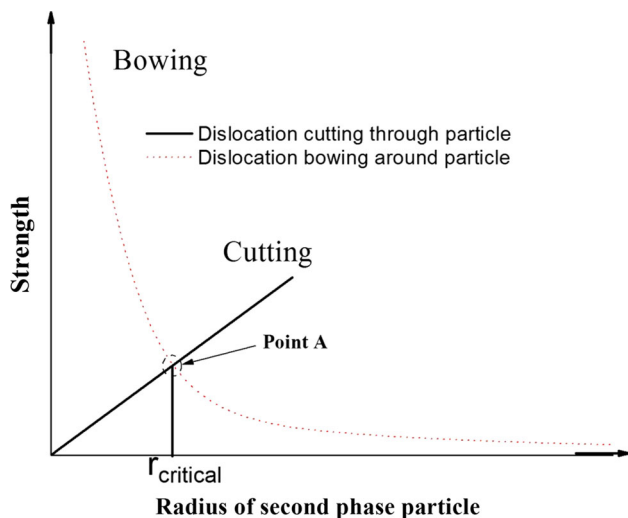


Fig. 3 The schematic diagram of material strength vs radius of the second-phase particle

anism in all conditions of this work was belonged to the bowing around particle mechanism, which represented the strength and hardness decreased with increasing ϵ -Cu particle size (Ref 1, 6). As the domain boundary migration became easier when the ϵ -Cu particle size increased, the activation energy of domain boundary migration (Q_a) became smaller when the ϵ -Cu particle size became bigger. Based on the calculated Q_a in different annealing temperature conditions, it can be concluded that during the 300 to 400 °C interval and 500 to 600 °C interval, the size of ϵ -Cu particles increases slowly. However, during the 400 to 500 °C interval, the size of ϵ -Cu particles increases quickly. It is reasonable to predict the maximum growth rate of ϵ -Cu particles occurring in 400 to 500 °C interval for 17-4PH, which is also confirmed by the previous work (Ref 1, 6).

Besides the growth behavior of domain size, the microstrain relaxation also takes place on the surface of peened 17-4PH during annealing process. The microstrain relaxation can also be obtained according to Voigt method. Figure 4 shows the evolution of surface microstrain in different annealing temperature conditions. It can be seen that microstrain decreases with increasing annealing time. The higher the annealing temperature is, the more obvious the microstrain relaxation will be. The microstrain relaxation rate is much higher at the initial stage and becomes lower with time increasing. The microstrain becomes 0.0016 when annealing 1 h with 600 °C, which is nearly the same as the microstrain of non-peened 17-4PH (Ref 21). According to the previous researches (Ref 28), the relaxation rate of microstrain $d\epsilon/dt$ can be given by:

$$\frac{d\epsilon}{dt} = -C\epsilon^m \exp\left[\frac{-Q_b}{RT}\right] \quad (\text{Eq 9})$$

where ϵ is the microstrain, m is the relaxation exponent, C is the material constant, and Q_b is the activation energy of microstrain relaxation. After integrating the ϵ , Eq 9 can be given as:

$$\epsilon_t^{-(m-1)} = \epsilon_0^{-(m-1)} + Ct(m-1) \exp\left[-\frac{Q_b}{RT}\right] \quad (\text{Eq 10})$$

where ϵ_0 is the original microstrain, and ϵ_t is the microstrain at t time. Based on Eq 10 and the data in Fig. 4, Q_b of annealing temperature 300, 400, 500 and 600 °C conditions

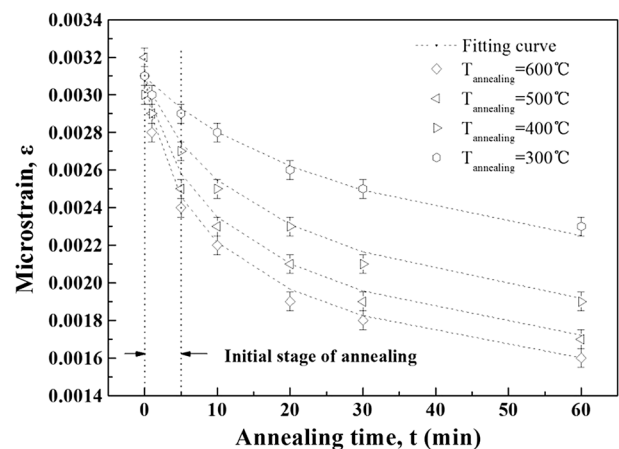


Fig. 4 The evolution of surface microstrain in different annealing temperature conditions

is obtained by computer regression analysis, which is 21.7, 21.6, 21.3 and 21.2 kJ/mol, respectively. From these calculated data, it can be seen that the microstrain relaxation activation energies in different annealing temperatures are nearly the same, which means the influence of annealing temperature on activation energy of microstrain relaxation is insignificant. Comparing the values of Q_a and Q_b in different annealing temperatures, it can be found that Q_a is much bigger than Q_b in all chosen temperatures. This result demonstrates that the occurrence of domain size growth behavior is more difficult than that of microstrain relaxation behavior.

In the annealing process of peened 17-4PH, domain size growth is due to the movement of grain and subgrain boundaries. The precipitation particles retard the domain growth through impeding the boundaries movements. Therefore, the effect of precipitation particles (ϵ -Cu) on the activation energy of domain boundary migration (Q_a) is remarkable when precipitation particle size changes. The microstrain relaxation is the recovery behavior during annealing process, which is determined by microstrain own property, and less influenced by the movement of grain and subgrain boundaries. Compared with the domain growth behavior, the microstrain relaxation behavior is less sensitive to precipitation size. Therefore, the value of Q_b , which is much smaller than the value of Q_a , changes unobviously with annealing temperature variation.

The evolution of surface dislocation density in different annealing temperature conditions is shown in Fig. 5. It can be seen that the value of dislocation density decreases sharply at the initial stage of annealing (5 min) and then decreases slightly. The higher the annealing temperature is, the more obvious this trend will be. Specifically, the ratios of the dislocation density decrement in the initial stage to the total decreased dislocation intensity during annealing process are about 72, 64, 32 and 31%, respectively, in the conditions of 600, 500, 400 and 300 °C annealing temperature. The effects of annealing temperature and time on dislocation density are both significant in 300, 400 and 500 °C. Comparing with the curves of 500 and 600 °C conditions, the difference between these two curves is not significant, which means the effect of annealing temperature on dislocation density becomes insignificant when annealing temperature is higher than 500 °C. From Fig. 5, it can be seen that the dislocation densities after 60-min annealing

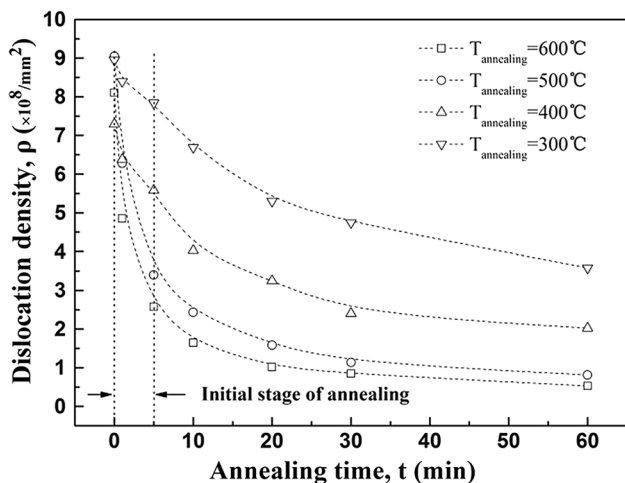


Fig. 5 The evolution of surface dislocation density in different annealing temperature conditions

via 600, 500, 400 and 300 °C annealing temperature are about $0.53 \times 10^8/\text{mm}^2$, $0.82 \times 10^8/\text{mm}^2$, $2.0 \times 10^8/\text{mm}^2$ and $3.6 \times 10^8/\text{mm}^2$, respectively. As we know that there is a certain amount of dislocation even in full annealing material, according to data from Fig. 5, it is reasonable to predict the dislocation density in full annealed 17-4PH is about $0.53 \times 10^8/\text{mm}^2$.

Besides investigating the surface recrystallization behavior, the recrystallization behavior of deformation layer in depth has also been investigated in this paper. In order to obtain the evolution of microstructure in deformation layer during annealing process, XRD analyses in depth were carried out in different annealing times. Figure 6 shows the depth profiles of domain size with different annealing times in 600 and 300 °C annealing temperature conditions. There is an obvious gradient distribution of domain size in depth direction after SP treatment, which is due to the impact energy decreasing with depth increasing. From Fig. 6(a), it can be seen that in the condition of 600 °C, domain sizes in different depth of deformation layer increase with increasing annealing time. Specifically, as the outside heat transfers to the top surface firstly during the annealing process, the domain size at top surface increases faster than that at subsurface, which makes a “hook region” in the D - δ curve when annealing time is less than 10 min. With annealing time

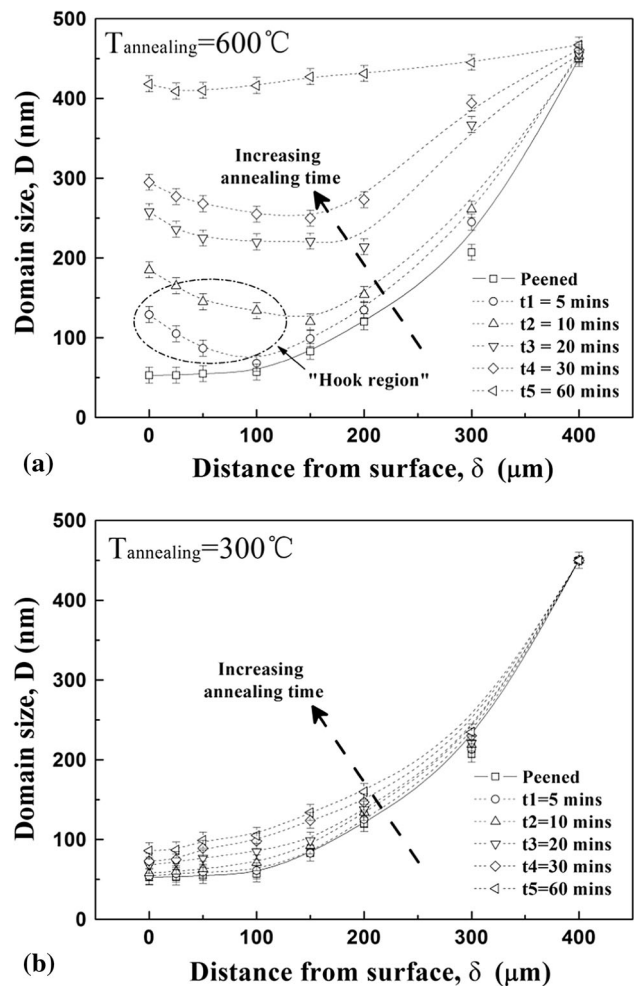


Fig. 6 The depth profiles of domain size with different annealing times in (a) $T_{\text{annealing}} = 600$ °C, (b) $T_{\text{annealing}} = 300$ °C annealing temperature conditions

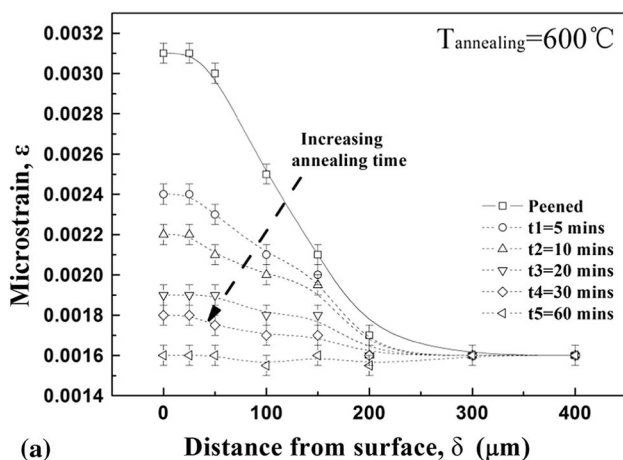
increasing, the temperature gradient in specimen becomes uniform and the D - δ curve becomes flatter. However, in the condition of 300 °C annealing process (Fig. 6b), the D - δ curves change very slightly with increasing annealing time, which represents the domain size nearly does not change in the whole deformation layer even if prolonging annealing time. Figure 7 shows the depth profiles of microstrain with different annealing times in 600 and 300 °C annealing temperature conditions. With the increase in annealing time, the microstrains in the whole deformation layer decrease. The higher the annealing temperature is, the more the relaxation of microstrain will be. Comparing with Fig. 6(b) and 7(b), it can be seen 300 °C annealing temperature only leads to the microstrain relaxation but nearly cannot lead to the domain size growth even if prolonging annealing time. However, in the condition of 600 °C, prolonging annealing time leads not only to the microstrain relaxation but also to the domain size growth in depth.

Additionally, the evolution of dislocation density in depth in 600 and 300 °C annealing temperature conditions can also be obtained according to the data in Fig. 6 and 7 via Eq 4, which are plotted in Fig. 8. It can be seen that the variation tendency of ρ - δ curve is in agreement with the variation tendency of ε - δ curve except for 5 and 10 min in 600 °C. The reason is due to the heat transfer from surface to interior as mentioned earlier. Dislocation density in the whole deformation layer decreases with increasing annealing temperature and time. Even in

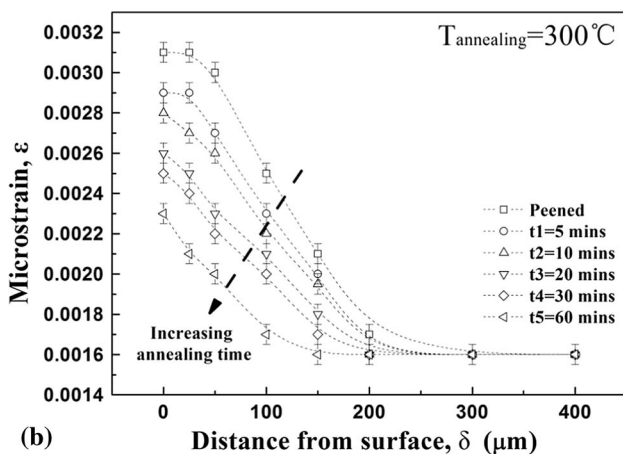
relative low annealing temperature such as 300 °C, the dislocation density decreases drastically (about 58% of total decrement in depth = 0 μ m and 39% of total decrement in depth = 200 μ m) after 60-min annealing time. It is well known that the interaction between dislocation such as dislocation intercross and dislocation tangle would increase the resistance of dislocation motion, which causes the increment of material yield strength. According to Bailey–Hirsch equation, the relationship between yield strength and dislocation density can be described as follows (Ref 29):

$$\sigma_s = \sigma_0 + \beta\mu b\rho^{1/2} \quad (\text{Eq 11})$$

where σ_0 is the yield strength of annealed material, β is a constant of material, μ is the shear modulus of material, and b is the Burgers vector of dislocations. From this equation, it can be seen that increasing dislocation density can increase the yield strength of materials. Work hardening process such as SP can increase the yield strength of surface region, which is another kind of strengthening mechanism of SP leading to better fatigue property (Ref 30). However, recrystallization behavior in annealing process alters the surface microstructure and mechanical property of peened materials. From Fig. 8, it can be concluded that the microstructure enhancement effect still exists in plastic deformation layer of peened 17-4PH

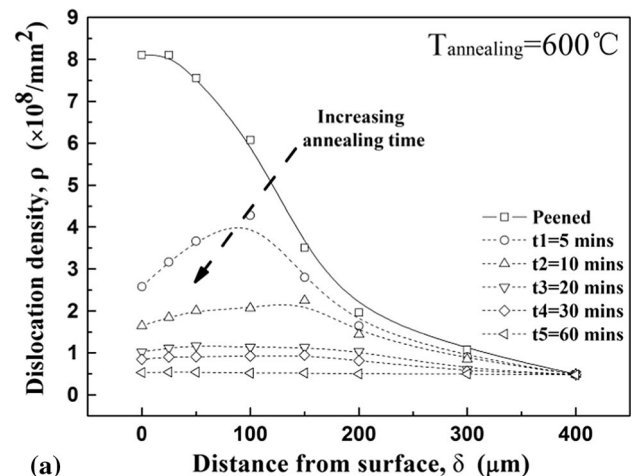


(a) Distance from surface, δ (μm)

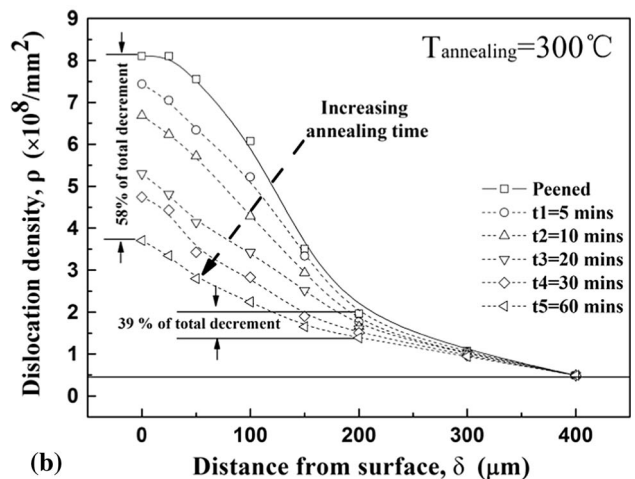


(b) Distance from surface, δ (μm)

Fig. 7 The depth profiles of microstrain with different annealing times in (a) $T_{\text{annealing}} = 600$ °C, (b) $T_{\text{annealing}} = 300$ °C annealing temperature conditions



(a) Distance from surface, δ (μm)



(b) Distance from surface, δ (μm)

Fig. 8 The depth profiles of dislocation density with different annealing times in (a) $T_{\text{annealing}} = 600$ °C, (b) $T_{\text{annealing}} = 300$ °C annealing temperature conditions

when 300 °C annealing temperature lasts for 60 min but nearly disappears when 600 °C annealing temperature lasts for 20 min.

4. Conclusions

The recrystallization behavior of surface deformation layer of 17-4PH introduced by shot peening was investigated via x-ray diffraction analysis in this work. The results reveal that with increasing time and temperature of isothermal annealing, domain size increases, but microstrain as well as dislocation density decrease. Because of the influence of precipitation particles on the movements of grain and subgrain boundaries, the activation energy of domain boundary migration (Q_a) decreases with increasing temperature of annealing process. Compared with growth behavior of domain size, microstrain relaxation behavior is less sensitive to precipitation particle size. Therefore, the activation energy of microstrain relaxation (Q_b) is nearly the same in different annealing temperatures but much smaller than Q_a . The maximum difference of Q_a between 400 and 500 °C annealing process shows the maximum growth rate of ϵ -Cu particles occurring in 400 to 500 °C interval. Additionally, according to the dislocation curve in different annealing temperature conditions, the effect of annealing temperature on dislocation density is significant in 300 to 500 °C interval, but insignificant in 500 to 600 °C interval. In terms of microstructure variation in depth, 300 °C annealing temperature can only change microstrain but nearly cannot change the domain size in the whole deformation layer even if prolonging annealing time. Dislocation density in the whole deformation layer decreases drastically if prolonging annealing time, no matter in 300 or 600 °C annealing process. Microstructure enhancement effect still exists in plastic deformation layer when 300 °C annealing temperature lasts for 60 min but nearly disappears when 600 °C annealing temperature lasts for 20 min.

Acknowledgments

The financial support of the National Natural Science Foundation of China (NSFC) (No. 51405356), the Research Fund for the Doctoral Program of Higher Education of China (No. 20130143120015) and State Key Laboratory of Materials Processing and Die & Mould Technology, Huazhong University of Science and Technology (P2016-06), are gratefully acknowledged.

References

1. C.N. Hsiao, C.S. Chiou, and J.R. Yang, Aging Reactions in 17-4PH Stainless Steel, *Mater. Chem. Phys.*, 2002, **74**, p 134–142
2. M.F. Yan, R.L. Liu, and D.L. Wu, Improving the Mechanical Properties of 17-4PH Stainless Steel by Low Temperature Plasma Surface Treatment, *Mater. Des.*, 2010, **31**, p 2270–2273
3. J. Yao, L. Wang, Q. Zhang, F. Kong, C. Lou, and Z. Chen, Surface Laser Alloying of 17-4PH Stainless Steel Steam Turbine Blades, *Opt. Laser Technol.*, 2008, **40**, p 838–843
4. Z. Wang, C. Jiang, X. Gan, Y. Chen, and V. Ji, Influence of Shot Peening on the Fatigue Life of Laser Hardened 17-4PH Steel, *Int. J. Fatigue*, 2011, **33**, p 549–556
5. Z. Wang, W. Luan, J. Huang, and C. Jiang, XRD Investigation of Microstructure Strengthening Mechanism of Shot Peening on Laser Hardened 17-4PH, *Mater. Sci. Eng., A*, 2011, **528**, p 6417–6425
6. Z. Wang, Y. Chen, and C. Jiang, Thermal Relaxation Behavior of Residual Stress in Laser Hardened 17-4PH Steel After Shot Peening Treatment, *Appl. Surf. Sci.*, 2011, **257**, p 9830–9835
7. R. Menig, V. Schulze, and O. Vöhringer, Comparison of Surface Characteristics and Thermal Residual Stress Relaxation of Laser Peened and Shot Peened AISI 4140, In: Wagner L, editor. Proceedings of the 8th International Conference on Shot Peening, Munich, 2002, p 498–504
8. V. Schulze, *Modern Mechanical Surface Treatment*, WILEY-VCH Verlag GmbH & Co. KGaA, Weinheim, 2006
9. W. Luan, C. Jiang, H. Wang, and J. Panardie, XRD Investigation of Thermostability of TiB₂/Al Deformation Layer Introduced by Shot Peening, *Mater. Sci. Eng., A*, 2008, **480**, p 1–4
10. H. Mirzadeh and A. Najafzadeh, Aging Kinetics of 17-4PH Stainless Steel, *Mater. Chem. Phys.*, 2009, **116**, p 119–124
11. E.A. Wilson, Quantification of Age Hardening in an Fe-12Ni-6Mn Alloy, *Scr. Mater.*, 1997, **36**, p 1179–1185
12. L.T. Shiang and C.M. Wayman, Maraging Behavior in an Fe-19.5Ni-5Mn Alloy I: Precipitation Characteristics, *Mater. Charact.*, 1997, **39**, p 529–553
13. T. Ungar and A. Borbely, The Effect of Dislocation Contrast on x-ray Line Broadening: A New Approach to Line Profile Analysis, *Appl. Phys. Lett.*, 1996, **69**, p 3173–3175
14. T. Ungar, I. Dragomir, A. Revesz, and A. Borbely, The Contrast Factors of Dislocations in Cubic Crystals: The Dislocation Model of Strain Anisotropy in Practice, *J. Appl. Crystallogr.*, 1999, **32**, p 992–1002
15. T. Ungar, Dislocation Densities, Arrangements and Character from X-ray Diffraction Experiments, *Mater. Sci. Eng., A*, 2001, **309–310**, p 14–22
16. S. Vives, E. Gaffet, and C. Meunier, X-ray Diffraction Line Profile Analysis of Iron Ball Milled Powders, *Mater. Sci. Eng., A*, 2004, **336**, p 229–238
17. J.I. Langford, A Rapid Method for Analysing the Breadths of Diffraction and Spectral Lines Using the Voigt Function, *J. Appl. Crystallogr.*, 1978, **11**, p 10–14
18. A.R. Stokes, A Numerical Fourier-Analysis Method for the Correction of Widths and Shapes of Lines on X-ray Powder Photographs, *Proc. Phys. Soc.*, 1948, **61**, p 382–391
19. G.K. Williamson and R.E. Smallman, Dislocation Densities in Some Annealed and Cold-Worked Metals from Measurements on the X-ray Debye-Scherrer Spectrum, *Philos. Mag.*, 1956, **1**, p 34–46
20. O. Vöhringer, Changes in the State of the Material by Shot Peening, In: H. Wohlfahrt, editor. Proceedings of the 8th International Conference on Shot Peening, Garmisch-Partenkirchen, Germany, 1987, p 185–204
21. Z. Wang, C. Jiang, X. Gan, and Y. Chen, Effect of Shot Peening on the Microstructure of Laser Hardened 17-4PH, *Appl. Surf. Sci.*, 2010, **257**, p 1154–1160
22. L. Xie, C. Jiang, W. Lu, K. Zhan, Q. Feng, X. Wu, and F. Wang, The Recrystallization Behavior of Surface Deformation Layer of (TiB + TiC)/Ti-6Al-4 V Composite During Isothermal Annealing, *Mater. Sci. Eng., A*, 2011, **530**, p 239–243
23. T. Roland, D. Rehrant, K. Lu, and J. Lu, Enhanced Mechanical Behavior of a Nanocrystallised Stainless Steel and Its Thermal Stability, *Mater. Sci. Eng., A*, 2007, **445–446**, p 281–288
24. J. Pan and J. Quan, *Fundamentals of Materials Science*, Tsinghua University Press, Beijing, 2002 ((in Chinese))
25. S.R. Goodman, S.S. Brenner, and J.R. Low, An FIM-Atom Probe Study of the Precipitation of Copper from Iron-1.4 at. pct Copper. Part II: Atom Probe Analyses, *Metall. Mater. Trans. B*, 1973, **4**, p 2371–2378
26. S.R. Goodman, S.S. Brenner, and J.R. Low, An FIM-Atom Probe Study of the Precipitation of Copper From Iron-1.4 at. pct Copper. Part I: Field-Ion Microscopy, *Metall. Mater. Trans. B*, 1973, **4**, p 2363–2369
27. W.D. Callister, *Fundamentals of Materials Science and Engineering*, 2nd ed., Wiley, Amsterdam, 2005
28. W. Luan, C. Jiang, and H. Wang, Investigation for Recrystallization Behavior of Shot Peened on TiB₂/6351Al Composite Using X-ray Diffraction, *Mater. Sci. Eng., A*, 2008, **496**, p 36–39
29. R.S. Liu and J.Y. Li, On the Structural Defects and Microscopic Mechanism of the High Strength of Amorphous Alloys, *Mater. Sci. Eng., A*, 1989, **114**, p 127–132
30. K. Dalaei, B. Karlsson, and L.E. Svensson, Stability of Shot Peening Induced Residual Stresses and Their Influence on Fatigue Lifetime, *Sci. Eng. A*, 2011, **528**, p 1008–1015